Macromolecules

ARTICLE

pubs.acs.org/Macromolecules

Biaxially Extended Thiophene−Fused Thiophene Conjugated Copolymers for High Performance Field Effect Transistors

Chih-Jung Lin,[†,§] Wen-Ya Lee,[†,‡,§] Chien Lu,[†] Hsiang-Wei Lin,[‡] and Wen-Chang Chen*[,†,‡]

[†]Department of Chemical Engineering, National Taiwan University, Taipei 106 Taiwan

[‡]Institute of Polymer Science and Engineering, National Taiwan University, Taipei 106 Taiwan

Supporting Information

ABSTRACT: We report the synthesis, properties, and field-effect transistor characteristics of biaxially extended thiophene-fused thiophene conjugated copolymers, **P4TDTT** and **P4TTT**, consisting of 2′,5″-5,5‴-di(2-ethylhexyl)-[2,3′;5′,2″;4″,2‴] -quaterthiophene and fused thiophene moieties of dithieno[3,2-*b*:2′,3′-*d*]thiophene and thieno[3,2-*b*]thiophene, respectively. The effect of fused thiophene size on the molecular packing and charge transport characteristics was explored. The high boiling point solvent facilitated the formation of ordered nanofiber morphology and enhanced the optoelectronic properties. **P4TDTT** exhibited a smaller *d*-spacing and $\pi-\pi$ stacking distance than **P4TTT** based and a denser nanofiber network. The optical band gaps of **P4TDTT** and **P4TTT** films spin-coated from trichlorobenezene (TCB) solvent were 1.84 and 1.86 eV, respectively. The highest hole mobilities of **P4TDTT** and **P4TTT** using TCB solvent were 0.610 and 0.396 $cm^2\ V^{-1}\ s^{-1}$, respectively, with the on/off ratios of 10^5-10^6. **P4TDTT** had better charge-transporting characteristics than **P4TTT** due to the nonsymmetry side-chain arrangement and larger coplanar moieties, leading to an enhanced interchain interaction and denser molecular packing. Furthermore, these polymers showed relatively high air stability due to the relative low-lying HOMO levels. This study revealed that the biaxially extended fused ring containing conjugated polythiophenes had excellent charge-transporting characteristics for FET applications.

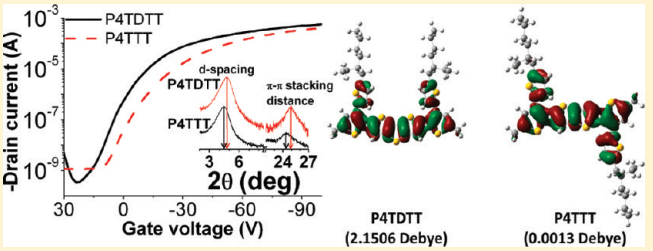

INTRODUCTION

Conjugated polymers have received extensive research in the field of field-effect transistors (FETs) due to their judicious chemical structures, flexibility, and solution processability.[1−9] Among conjugated polymers, poly(3-hexyl thiophene) (P3HT) was considered as a promising material for solution-processed organic FETs, because of the high hole mobility of 0.01−0.1 $cm^2\ V^{-1}\ s^{-1}$.[10−12] However, the performance of the P3HT devices showed a dramatic degradation after exposure to the air,[13] because of its high HOMO energy level(−4.8 eV).[14] The poor ambient stability restricted the practical application of the P3HT devices. One of the effective methodologies to increase the air stability was to lower the HOMO energy level by balancing the backbone coplanarity and FET functionality.[15−21] For example, conjugated polymers with conjugated side chains were shown to reduce the HOMO energy level (−5.46 to −5.62 eV) by steric hindrance,[18−21] in comparison with those of parent P3HT. In addition, conjugated side chains are capable of extending the delocalization of π electrons into the main chains, thus enhancing strong intermolecular interaction. Despite the good air stability, the mobilities of the reported biaxially extended thiophene donor-based polymers were commonly in the range from 10^{-2} to 10^{-4} $cm^2\ V^{-1}\ s^{-1}$,[18,22−24] insufficient for the commercial applications of FETs. The FET mobility of the above conjugated polymers could be enhanced by crystalline-induced structure, such as incorporating fused thiophene ring moiety.[25−47]

The fused thiophene rings possesses a highly planar system, allowing a small $\pi-\pi$ stacking distance. The highly coplanar conformation also induced the formation of highly ordered crystalline structure, significantly promoting charge transporting ability.[31,35,39,40] Fused-thiophene-based conjugated polymers, such as poly(2,6-bis(3-alkylthiophen-2-yl)dithieno[3,2-*b*:2′,3′-*d*]-thiophene) (PBTDT)[35,48] and poly(2,5-bis(3-alkylthiophen-2-yl)-thieno[3,2-*b*]thiophenes) (PBTTT),[39,40] exhibited hole mobilities larger than 0.1 $cm^2\ V^{-1}\ s^{-1}$, higher than the parent P3HT. It would be of interest to incorporate fused-thiophene ring into biaxially extended thiophene conjugated polymers for exploring the morphology and FET applications.

Herein, we report high-performance air-stable FETs based on two biaxially extended thiophene-fused thiophene containing conjugated polymers, poly(2′,5″-5,5‴-di(2-ethylhexyl)-[2,3′;5′,2″;4″,2‴]quaterthiophene-*alt*-2,6 -dithieno[3,2-*b*:2′,3′-*d*]-thiophene)(**P4TDTT**) and poly(2′,5″-5,5‴-di(2-ethylhexyl) -[2,3′;5′,2″;4″,2‴]quaterthiophene-*alt*-2,5-thieno[3,2-*b*]thiophene) (**P4TTT**). These polymers were synthesized by Stille coupling

Received: September 5, 2011
Revised: November 6, 2011
Published: November 30, 2011

Scheme 1. Synthetic Scheme of P4TTT and P4TDTT

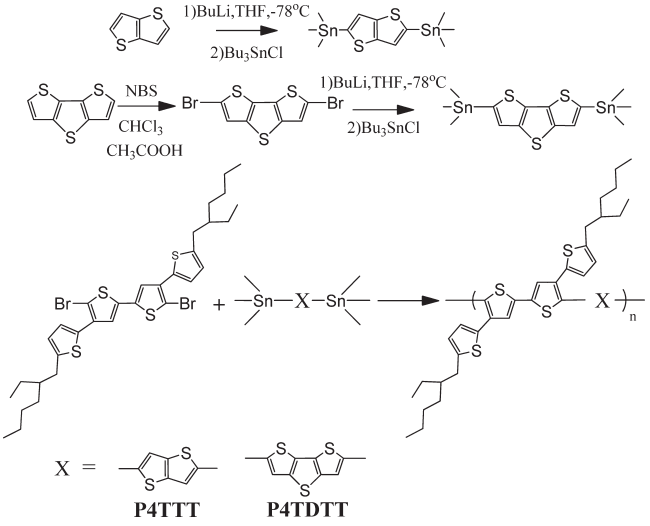

reaction under microwave heating, as shown in Scheme 1. To elucidate the effect of fused thiophene size on the molecular packing and charge transport, two core sizes of the fused-thiophene-ring structures were incorporated into the main chain, including dithienothiophene (**DTT**) and thienothiophene (**TT**). The morphology of the prepared conjugated polymers was studied by X-ray diffraction (XRD) and transmission electron microscope (TEM). The polymer carrier mobility was obtained from the top-contact/bottom-gate field effect transistor (FET) devices and correlated with the morphology. The experimental results suggested the incorporation of the fused thiophene ring into the biaxially extended thiophene conjugated polymers significantly enhanced the FET mobility as well as their air stability.

EXPERIMENTAL SECTION

Synthesis. The monomers, 2,6-Bis(tri-*n*-butylstannyl)-dithieno[3,2-*b*:2′,3′-*d*]-thiophene (**DTT**), 2,5-Bis(tri-*n*-butylstannyl)thieno[3,2-*b*]-thiophene (**TT**) and 2′,5″-dibromo-5,5‴-di-(2-ethylhexyl)-[2,3′;5′,2″;4″,2‴]-quaterthiophene ($4TBr_2$) were synthesized according to the literature methods.[19−21,39,49,50] The general procedure of synthesizing conjugated copolymer **P4TDTT** and **P4TTT** are shown in Scheme 1. $4TBr_2$, fused thiophene rings monomers (**DTT** and **TT**), tri(*o*-tolyl)-phosphine (16 mol %, with respect to the monomers), and tris-(dibenzylideneacetone)dipalladium(0) (2 mol % with respect to the monomers) were dissolved in anhydrous chlorobenzene and the copolymer was synthesized by Pd(0)-catalyzed Stille coupling polymerization under microwave heating for 2 h. After that, it was end-capped with 2-(tributylstynnyl)thiophene and 2-bromothiophene (both 1.1 equiv with respect to ditin monomer), the mixture was cooled and poured into hexane. The precipitated material was dissolved into a small amount of chloroform and then reprecipitated into methanol. The crude polymer was purified further by washing for 3 days in a Soxhlet apparatus with methanol, acetone and hexane to remove oligomers and catalyst residues. The final product was obtained after drying in vacuum at 40 °C. The chemical structures of the synthesized polymers were confirmed by ^{1}H NMR (shown in Figure S1) and elemental analysis.

Poly(2′,5″-5,5‴-di(2-ethylhexyl)-[2,3′;5′,2″;4″,2‴]quaterthiophene-*alt*-2,6-dithieno[3,2-*b*:2′,3′-*d*]thiophene) (**P4TDTT**). 426 mg (0.6 mmol) of the $4TBr_2$, 314 mg (0.6 mmol) of the **DTT**, and 5 mL anhydrous chlorobenzene were used to afford a black solid (yield: 72%). ^{1}H NMR ($CDCl_3$), δ (ppm): 7.21−7.19 (br, Ar−H, 1H),7.19−7.10 (br, Ar−H, 1H), 7.00−6.90 (br, Ar−H, 1H), 6.70−6.60 (br, Ar−H, 1H), 2.80−2.67 (br, Ar−CH_2, 2H), 1.49−1.05 (br, −CH and −CH_2, 9H), 0.95−0.70 (br, −CH_3, 6H). Anal. Calcd for [$C_{40}H_{43}S_7$]: C, 64.21; H,5.79; S, 30.00. Found: C, 63.77; H,5.55; S, 29.98.

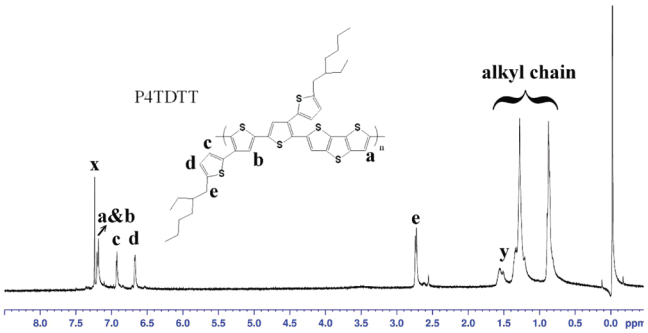

Figure 1. ^{1}H NMR spectra of **P4TDTT** in $CDCl_3$. (*x*, $CDCl_3$; *y*, H_2O).

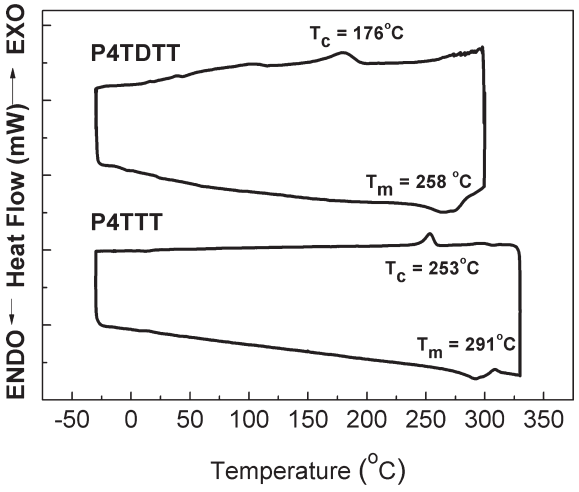

Figure 2. DSC curves of **P4TDTT** and **P4TTT** at the heating rate of 5 °C/min under a nitrogen atmosphere.

Poly(2′,5″-5,5‴-di(2-ethylhexyl)-[2,3′;5′,2″;4″,2‴]quaterthiophene-*alt*-2,5-thieno[3,2-*b*]thiophene) (**P4TTT**). 284 mg (0.61 mmol) TT, 435 mg (0.61 mmol) 4T-Br_2, and 5 mL chlorobenzene were used to afford a black solid (yield: 52%). ^{1}H NMR ($CDCl_3$), δ (ppm): 7.40−7.26 (br, Ar−H, 1H),7.22−7.10 (br, Ar−H, 1H), 7.00−6.90(br, Ar−H, 1H), 6.70−6.60 (br, Ar−H, 1H), 2.80−2.67 (br, Ar−CH_2, 2H), 1.49−1.10 (br, −CH and −CH_2, 9H), 0.95−0.65 (br, −CH_3, 6H). Anal. Calcd for [C38H42S6]: C, 66.04; H, 6.13; S, 27.84. Found: C, 65.84; H, 6.07; S, 27.80.

Characterization. ^{1}H NMR spectra were recorded with a Bruker Avance DRX 400 MHz instrument. Gel permeation chromatographic (GPC) analysis was performed on a Lab Alliance RI2000 instrument (two column, MIXED-C and D from Polymer Laboratories) which was connected to one refractive index detector from Schambeck SFD Gmbh. All GPC analyses were performed in polymer/THF solution at a flow rate of 1 mL/min at 40 °C and calibrated with polystyrene standards.

Thermogravimetric analysis (TGA) and differential scanning calorimetry (DSC) measurements were measured under a nitrogen atmosphere at a heating rate of 10 and 5 °C per minutes by using a TA Instruments (TGA-951 and DSC-910S, respectively). Cyclic voltammetry (CV) was performed with the use of a three-electrode cell in which ITO was used as a working electrode, and the polymer film was coated on it in 0.5 × 0.7 cm^2. A platinum wire was used as an auxiliary

dx.doi.org/10.1021/ma202017q |*Macromolecules* 2011, 44, 9565–9573

electrode. All cell potentials were taken with the use of a homemade Ag/AgCl, KCl (sat.) reference electrode. UV−vis absorption spectra were measured with Hitachi U4100 spectrophotometer. X-ray diffraction (XRD) was performed by Rigaku TTRAX 3 diffractometer using Cu Kα radiation (λ = 1.5418 Å) with a typical scan range of 2−30°. Transmission electron microscope (TEM) images were obtained with JEOL JEM-1230 operated at 100 kV with a GATAN DualVision CCD. For XRD, UV, and TEM, the conditions of polymer samples are the same with the device fabrication.

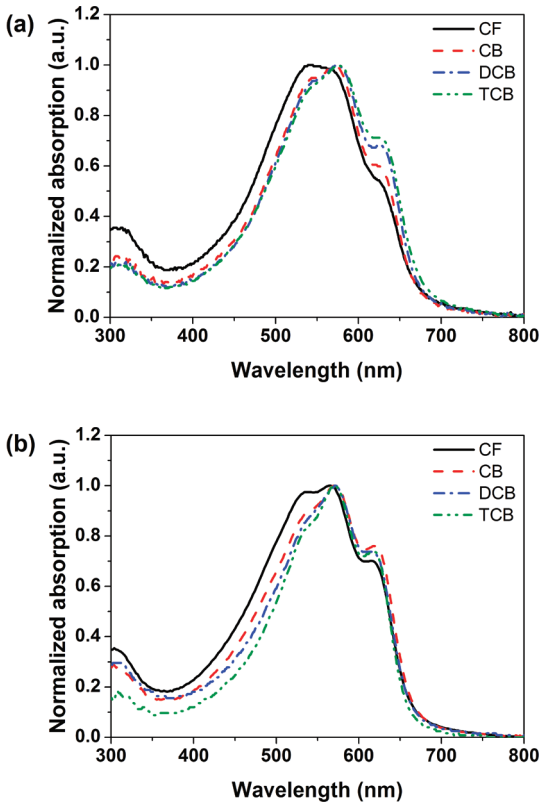

Figure 3. Normalized absorption spectra of (a) **P4TDTT** and (b) **P4TTT** thin films prepared from CF, CB, DCB, and TCB.

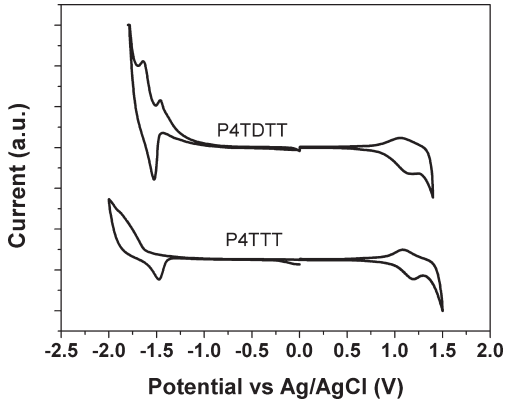

Figure 4. Cyclic voltammograms of **P4TDTT** and **P4TTT** thin films in an acetonitrile solution of 0.1 M TBAP at a scan rate of 0.1 V/s.

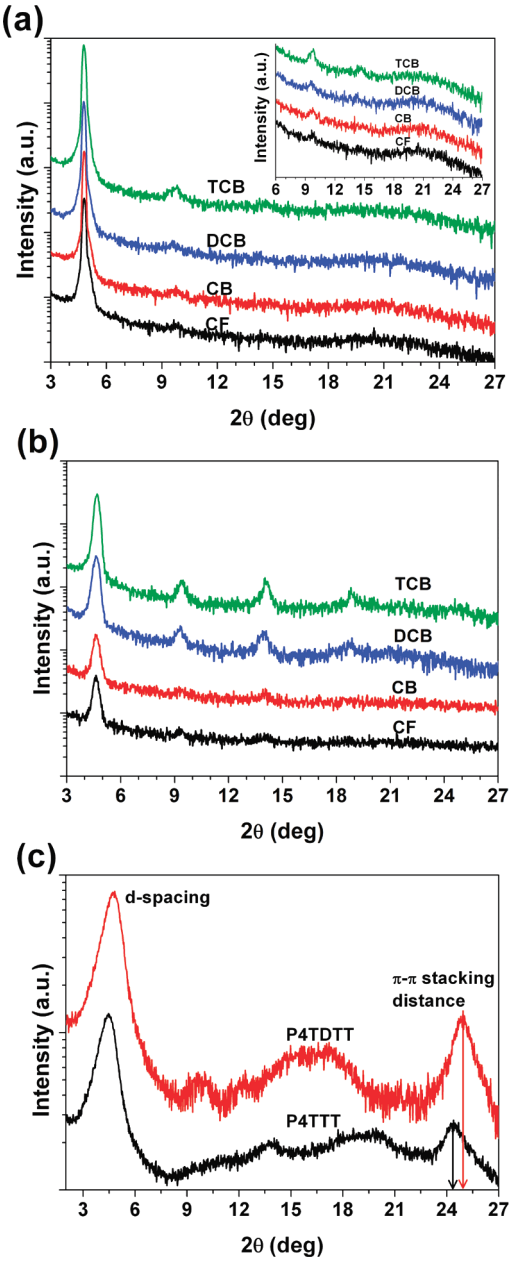

Figure 5. XRD profiles of (a) **P4TDTT** and (b) **P4TTT** thin films. (c) XRD profiles of **P4TDTT** and **P4TTT** powders. The inset figure is the magnified XRD patterns from 2θ = 6−27°.

Table 1. Thermal, Electronic, and Electrochemical Properties of P4TDTT and P4TTT

	UV−vis absorption		Cyclic Voltammetry				
polymer	λ_{max} (nm)[a]	E_g^{opt} (eV)[a]	E^{ox}_{onset} (V)	HOMO (eV)	E^{red}_{onset} (V)	LUMO (eV)	E_g^{ec} (eV)
P4TDTT	542, 576, 627	1.84	0.82	−5.14	−1.22	−3.1	2.04
P4TTT	537, 571, 620	1.86	0.97	−5.29	−1.27	−3.05	2.24

[a] The data were obtained from the thin films prepared from TCB.

dx.doi.org/10.1021/ma202017q |*Macromolecules* 2011, 44, 9565–9573

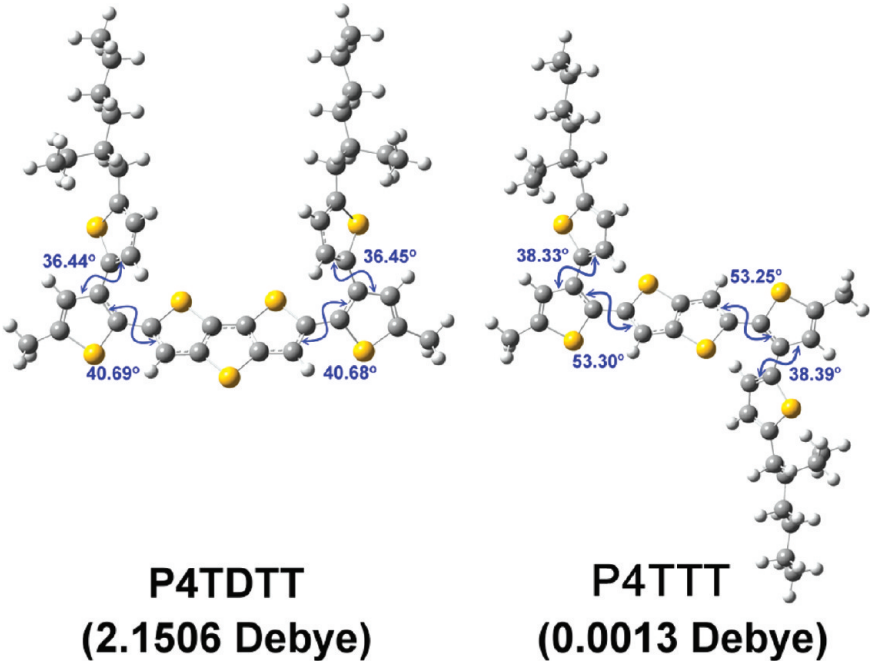

Figure 6. Optimized geometries of **P4TDTT** and **P4TTT** by the Gaussian 03 program using DFT//B3LYP/6-31G(d) method.

The surface morphologies of polymer film surface were also studied by AFM (Figure S4, Supporting Information) using a Nanoscope 3D Controller (AFM, Digital Instruments) operated in tapping mode at room temperature. For AFM samples, 5 mg mL^{-1} polymer solution in 1,2,4-trichlorobenzene was filtered through a 0.22 μm syringe filters, and then spin-coated at a speed rate of 500 rpm for 600 s onto the octadecyltrichlorosilane-treated SiO_2/Si substrates. The thin film samples for TEM characterizations were prepared by spin-coating at a speed rate of 500 rpm for 600 s on copper grids with carbon, which was fixed on a glass slide. Sequentially the samples were annealed at 200 °C (for **P4TDTT**) and 260 °C (for **P4TTT**) for 60 min in a N_2-filled glovebox. After thermal annealing, the TEM samples were peeled from glass slide. The beam current is under 511 μA, and the voltage is 100 kV. Note that all the samples for TEM characterizations were measured without staining. The thickness of the P4TDTT and P4TTT thin films are 65 and 75 nm, respectively. The thickness of the polymer films was measured with a microfigure measuring instrument (Surfcorder ET3000, Kosaka Laboratory Ltd.).

Computational Methodology. Theoretical molecular simulation of the oligoimides was calculated through Gaussian 03 program package. Density functional theory (DFT) method using Becke's three-parameter functional with the Lee, Yang, and Parr correlation functional method (B3LYP) with 6-31G(d) was exploited for the optimization of ground-state molecular geometry.[51]

Fabrication and Characterization of FETs. The FET devices using the heavily doped (n^+) silicon (100) wafer as the substrate and a 200 nm SiO_2 layer as the gate insulator were thermally grown onto the silicon wafer. Prior to surface treatments, wafer and quartz glass were cleaned by piranha solution (7:3 mixture of H_2SO_4 and H_2O_2) and then rinsed with deionized water at least 6 times. The surface treatments on SiO_2/Si substrates were obtained by the following procedure: a clean SiO_2/Si substrate was immersed into a 10 mM solution of octadecyltrichlorosilane (ODTS) in anhydrous toluene at 80 °C for 3 h under N_2-filled environment. Polymer solution (5 mg mL^{-1}) dissolved in anhydrous chlorinated solvents at 120 °C for 1 h to make sure the polymer dissolved well. The dissolved solution was slowly cooled down to room temperature for 2 h. The thin film was spin-coated at 500 rpm for 600 s onto the ODTS-treated SiO_2/Si substrate and annealed at 200 °C (for **P4TDTT**) and 260 °C (for **P4TTT**) for 60 min in a N_2-filled glovebox. The top-contact source and drain electrode were defined by a 100 nm-thick Au layer through a regular shadow mask, and the channel length (L) and width (W) were 50 and 1000 μm, respectively. Output and transfer characteristics of the TFTs were measured using a Keithley 4200 semiconductor parametric analyzer. All of the electronic measurements were measured in N_2-filled glovebox. The field effect mobility (μ_{sat}) was measured by the transfer curves in the saturation regime and estimated by eq 1:[3,9,52,53]

$$I_{ds,\,sat} = \frac{WC_i}{2L}\mu_{sat}(V_{gs} - V_t)^2 \quad (1)$$

Here W and L are channel width and length, respectively, C_i is the capacitance of gate insulator, and V_t is a threshold voltage. μ_{sat} is a carrier mobility determined from the slope of $(-I_{ds})^{1/2}$ versus V_{gs} in the saturation regime.

RESULTS AND DISCUSSION

P4TDTT and **P4TTT** were prepared by the Stille coupling reaction under microwave heating, as shown in Scheme 1. The chemical structures of the synthesized polymers were confirmed by ^{1}H NMR and elemental analysis. Figure 1 shows the ^{1}H NMR spectrum of **P4TDTT** in $CDCl_3$. For aromatic protons, the three peaks at 7.18 (peak b), 6.93 (peak c), and 6.67 (peak d) ppm are assigned to the protons on the thiophene rings of **4T** unit,[19] while the peak at 7.20 (peak a) ppm refers to the proton on the **DTT** segment.[35] Moreover, the peaks at 1.49−1.10 (−CH and $-CH_2$, 9H) and 0.95−0.65 ($-CH_3$, 6H) are attributed to the ethylhexyl group in the **4T** moiety. The number of aromatic and aliphatic protons estimated from the integration of peak is in a good agreement with the proposed polymer structures. The ^{1}H NMR spectra of the **P4TTT** is also consistent with the proposed polymer structures, as shown in Figure S1 in the Supporting Information. Besides, the experimental carbon, hydrogen, and nitrogen contents of the studied polymers are in a good agreement

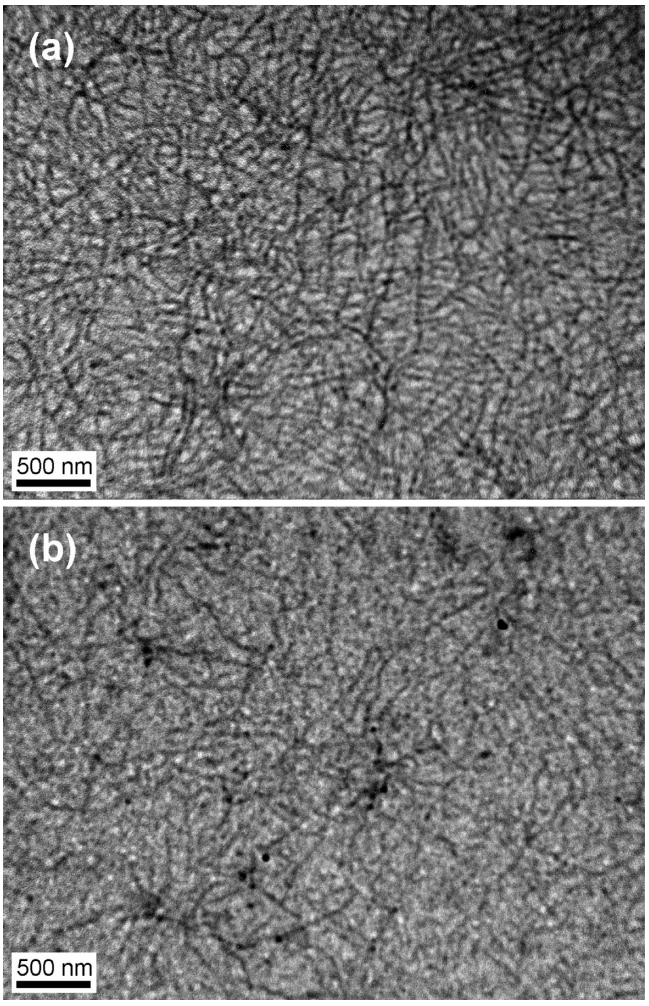

Figure 7. TEM images of (a) **P4TDTT** and (a) **P4TTT** thin films prepared from TCB.

with the theoretical values. The above structural characterization indicates the successful synthesis of the biaxially extended fused-thiophene conjugated copolymers.

Both polymers are soluble in chlorinated solvents and could be spin-coated into uniform thin films for FET applications, such as chloroform (CF), chlorobenzene (CB), 1,2-dichlorobenzene (DCB), and 1,2,4-trichlorobenzene (TCB). **P4TDTT** and **P4TTT** have the weight-average molecular weights of 9450 and 8740 using THF as the GPC solvent, respectively, with the polydispersity indexes of 1.39 and 1.28. The molecular weights of **P4TDTT** and **P4TTT** might be underestimated, because they were partial soluble in THF.

The thermal properties of **P4TDTT** and **P4TTT** were evaluated by the curves of thermogravimetric analysis (TGA) (Figure S2 of the Supporting Information) and differential scanning calorimetry (DSC) (Figure 2). The TGA curves of **P4TTT** and **P4TDTT** revealed the thermal decomposition temperatures (T_d, 95 wt % residue) of 429 and 465 °C, respectively, showing a good thermal stability. **P4TDTT** and **P4TTT** exhibited the crystallization and melting temperatures (T_c, T_m) of (176, 258) and (253, 291) °C, respectively. The crystalline **P4TDTT** and **P4TTT** may have good interchain π−interaction for achieving a high FET mobility.

Figure 3 shows the UV−vis absorption spectra of **P4TDTT** and **P4TTT** thin films prepared from the various boiling-point solvents, including chloroform (CF, bp = 60 °C), chlorobenzene (CB, bp = 132 °C), 1,2-dichlorobenzene (*o*-DCB, bp = 174 °C) and 1,2,4-trichlorobenzene (TCB, bp = 214 °C). The absorption maxima of thin films of **P4TDTT** and **P4TTT** with using various solvents (CF, CB, DCB and TCB) after thermal annealing are (542, 570, 576, 576) and (566, 571, 571 571) nm, respectively. These λ_{max} exhibited obvious bathochromic shifts with using higher boiling point solvents, such as TCB. It indicates that higher boiling-point solvent provides a longer dry time to facilitate the chain packing and interchain π−electron interaction. The UV−vis spectra of **P4TDTT** and **P4TTT** thin films prepared from TCB respectively showed three well-defined vibronic peaks. The stronger absorption peaks at 627 and 620 nm, corresponding to the higher interchain π−π stacking using TCB,[35] as compared with those made from low-boiling-point CF. The optical band gaps of **P4TDTT** and **P4TTT** films (using TCB solvent) estimated from the absorption edges are 1.84 and 1.86 eV, respectively. **P4TDTT** shows a smaller band gap than **P4TTT**, presumably due to the three-member fused rings with a longer conjugation length. Theλ_{max} of **P4TDTT** (576 nm) and **P4TTT** (571 nm) thin films exhibited significant bathochromic shifts, compared to those of PBTDT (558 nm)[35] and PBTTT (547 nm) reported in the literature.[39] These shifts may be attributed to the extended delocalization of π electrons from pendant thienyl moieties into the polymer backbone.[18]

Figure 4 shows the cyclic voltammagrams of **P4TDTT** and **P4TTT**. The details of electrochemical properties are summarized in Table 1. These polymers exhibit reversible p-doping/dedoping and n-doping/dedoping processes. Note that the reduction peaks at −1.45 V is attributed to the reduction reaction of H_2O.[54] The reduction peak of P4TDTT is −1.65 V. The HOMO and LUMO energy levels were estimated from onset oxidation potentials (E^{ox}_{onset}) and onset reduction potentials (E^{red}_{onset}) based on the following equations:[52,53] $E_{HOMO} = -[E^{OX}_{onset} - E^{ferrocene}_{1/2} + 4.8]$ V and $E_{LUMO} = -[E^{red}_{onset} - E^{ferrocene}_{1/2} + 4.8]$ V, where the potential was referred to an Ag/AgCl reference electrode.[19] The obtained HOMO energy levels of **P4TDTT** and **P4TTT** are −5.14 and −5.29 eV, respectively, and the LUMO energy levels are −3.10 and −3.05 eV. The HOMO levels of **P4TDTT** and **P4TTT**, are 0.34 and 0.49 eV lower than that of P3HT (−4.8 eV),[14] respectively, which is expected to improve the air stability of the performance of devices. The trend of these optical band gaps is consistent with that of the electrochemical band gaps of **P4TDTT** (2.04 eV) and **P4TTT** (2.24 eV). It should be noted that the electrochemical band gap larger than the optical band gaps is related to the exciton binding energy of the conjugated polymers.[55]

X-ray diffraction (XRD) was used to investigate the molecular packing of the studied polymers. Parts a and b of Figure 5 show the XRD profiles of **P4TDTT** and **P4TTT** thin films prepared from the different solvents after thermal annealing. The XRD patterns of **P4TDTT** and **P4TTT** prepared from TCB exhibit well-defined (100), (200), (300) peaks at (4.78°, 9.82°, 14.60°) and (4.69°, 9.47°, 14.03°), whereas the (200) and (300) peaks of the films coated from CF are significantly suppressed. These results may be resulted from the fact that the high boiling-point solvent provided a long dry time for the polymer chains to self-assembly a thermodynamically favored packing.[56] It is worth noting that **P4TTT** showed the fourth diffraction peak at 18.81°. This high order peak may suggest that the **P4TTT** thin films

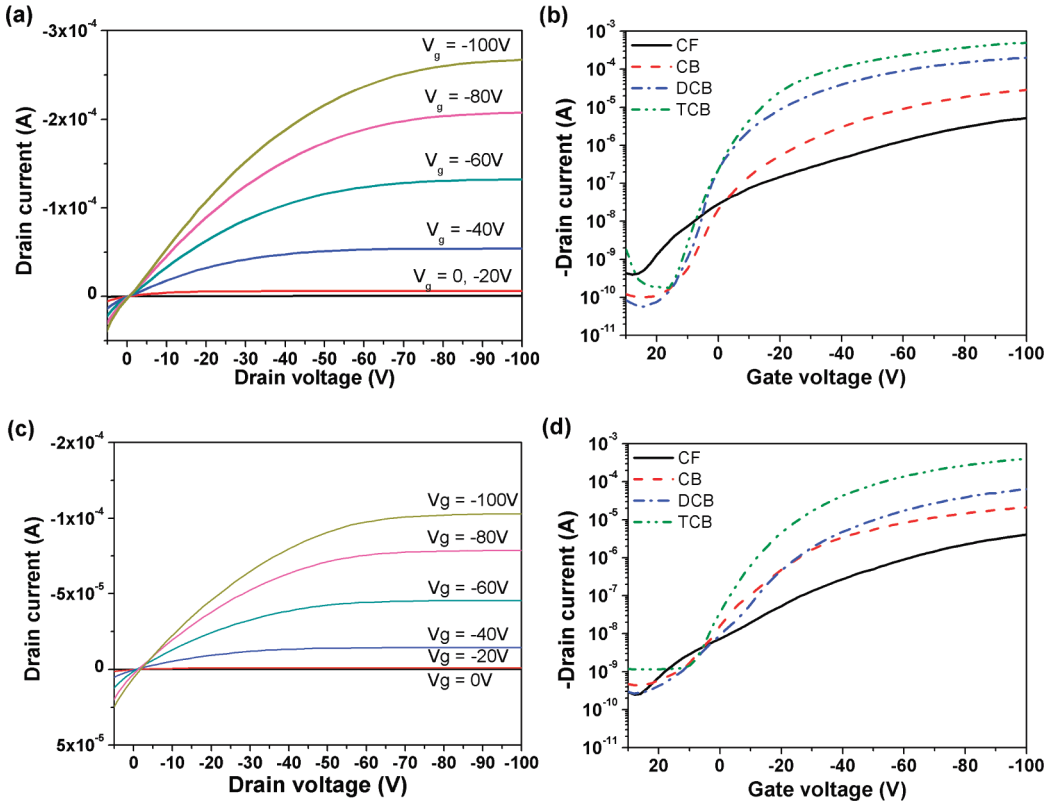

Figure 8. Output and transfer characteristics of the FETs prepared from (a,b) **P4TDTT** and (c,d) **P4TTT**.

possess higher extent of molecular layering, compared to **P4TDTT**. The **P4TDTT** and **P4TTT** thin films exhibit different interchain *d*-spacing of 18.48 and 18.83 Å, as estimated from XRD profiles. It indicates that the number of fused-thiophene rings had significant effects on the molecules packing.[29,37,57] The XRD patterns (Figure 5c) on the **P4TDTT** and **P4TTT** powders display two diffraction peaks at 2θ = (4.82°, 25.02°) and (4.46°, 24.38°), respectively, corresponding to the side-chain *d*-spacing and $\pi-\pi$ stacking distance of these polymers. The estimated side-chain *d*-spacing and $\pi-\pi$ stacking distance of **P4TDTT** and **P4TTT** are (18.32 Å, 3.56 Å) and (19.80 Å, 3.65 Å), respectively. **P4TDTT** has a smaller *d*-spacing and $\pi-\pi$ stacking distance than **P4TTT**, implying that the former possesses a denser structure. This is probably due to the fact that **P4TDTT** has larger coplanar moieties than **P4TTT**.

Figure 6 shows the optimization of molecule geometries of these polymers obtained by the Gaussian 03 program using DFT//B3LYP/6-31G(d) method. The dihedral angle between the conjugated backbone and the side-chain thienyl moieties of **P4TDTT** and **P4TTT** are 40° and 53°, respectively. On the other hand, the dihedral angles of between thiophene units and fused-thiophene rings of **P4TDTT** and **P4TTT** are 36° and 39°, respectively. The distorted conformation of these polymers is probably attributed to the intramolecular repulsion from the sulfur atoms.[18] The large core size of fused-thiophene rings on **P4TDTT** offers more space to reduce the repulsion force between the neighbor bulky side-chain groups. Therefore, **P4TDTT** shows a more coplanar backbone conformation and better molecular packing of polymer chains, as evidenced by the XRD results. The dipole moments of these polymers were also estimated. The estimated dipole moments of **P4TDTT** (2.1506 D) is much larger than that of **P4TTT** (0.0013 D). The optimized theoretical geometry of **P4TDTT** has two conjugated side chains on the same side, whereas that of **P4TTT** has one side chain on the each side. The nonsymmetry side-chain arrangement of **P4TDTT** results in a large dipole moment and a stronger interchain interaction, enhancing the molecular packing.[58,59] Note that the prepared biaxially extended thiophene-fused thiophene polymers present smaller $\pi-\pi$ stacking distances in comparison to PBTDT and PBTTT.[35,39] It suggests that the conjugation side chains not only increase the π-electron density in the main chain, but also enhance the $\pi-\pi$ interaction, leading to a denser stacking.

Figure 7 shows TEM images of the polymer films prepared from the TCB solutions. The images of **P4TDTT** and **P4TTT** thin films exhibit a well-defined nanofiber morphology with an average diameter of around 40 nm. Furthermore, **P4TDTT** thin film shows a denser network of nanofibers than **P4TTT**, presumably due to the higher coplanarity and strong intermolecular interaction. The dense nanofiber morphology of **P4TDTT** is capable of benefiting charge transport since it provides effective channels for carrier transporting.[60,61] However, the nanofiber morphology is significantly suppressed when the low-boiling-point solvent is used as a processing solvent (Figure S3 in the Supporting Information), due to an insufficient deposition time for the aggregation of polymer chains. Furthermore, we investigate the AFM topography images of the **P4TDTT** and **P4TTT** thin films, as shown in Figure S4 of Supporting Information. These two samples also show the fibrillar morphologies. These results also support that the P4TDTT and P4TTT thin films possessed the nanofiber morphology.

Field-effect transistors (FETs) were fabricated by spin-coated thin films on the octadecyltrichlorosilane (ODTS)-modified

dx.doi.org/10.1021/ma202017q |*Macromolecules* 2011, 44, 9565–9573

Table 2. Electrical Characteristics of the P4TTT and P4TDTT FETs Fabricated from Different Solvents[a]

polymer	solvent	mobility^{max} ($cm^2\ V^{-1}\ s^{-1}$)	mobility^{avg} ($cm^2\ V^{-1}\ s^{-1}$)	$I_{on}/I_{off}{}^{avg}$	$V_t{}^{avg}$ (V)
P4TDTT	CF	0.005	$(4.66 \pm 0\,0.39) \times 10^{-3}$	1.21×10^4	−16
	CB	0.034	$(2.24 \pm 0\,0.87) \times 10^{-2}$	1.46×10^6	−15
	DCB	0.154	$(1.19 \pm 0\,0.32) \times 10^{-1}$	1.52×10^5	−3
	TCB	0.610	$(5.58 \pm 0\,0.65) \times 10^{-1}$	1.98×10^6	−2
P4TTT	CF	0.0049	$(4.10 \pm 0\,0.84) \times 10^{-3}$	1.57×10^4	−19
	CB	0.028	$(2.20 \pm 0\,0.57) \times 10^{-2}$	5.37×10^4	−12
	DCB	0.093	$(8.51 \pm 0\,0.81) \times 10^{-2}$	1.05×10^5	−18
	TCB	0.306	$(3.04 \pm 0\,0.50) \times 10^{-1}$	7.45×10^5	−13

[a] The average values were obtained for at least 20 devices from 3 batches.

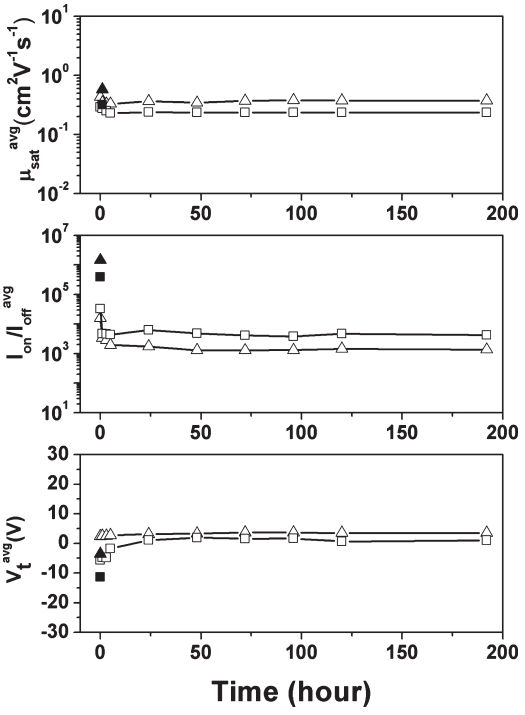

Figure 9. Air stability testing of the **P4TDTT** (up triangle) and **P4TTT** (square)_FETs, including hole mobility (μ_{sat}), on/off ratio (I_{on}/I_{off}), and threshold voltage (V_t). The solid symbols correspond to an electrical performance in a nitrogen-purging glovebox. Relative humidity ranges from 50 to 60% in air.

SiO_2/Si substrates. Figure 8 shows the FET performance based on **P4TDTT** and **P4TTT** with thermal annealing at 200 °C (for **P4TDTT**) and 260 °C (for **P4TTT**) for 60 min under a dark environment in N_2-filled glovebox. The details of the electrical properties are summarized in Table 2. The FET output characteristics based on **P4TDTT** and **P4TTT** exhibit good current modulation and well-defined saturation regions, as shown in Figure 8, parts a and c. Furthermore, the corresponding transfer characteristics of the FETs prepared from the different solvents are shown in Figure 8, parts b and d. The average values of the performance of the FETs were obtained for at least 20 devices from 3 different batches. The FET hole mobilities largely increases with the elevated boiling point of the solvents. The trend of the mobilities is consistent with that of the above XRD results. The hole mobility of **P4TDTT** prepared from TCB is 2 orders of magnitude higher than that prepared from CF. The maximum FET mobility (0.61 $cm^2\ V^{-1}s^{-1}$), the highest on−off ratio (1.98×10^6) and the lowest threshold voltage (−2 V) of **P4TDTT** are obtained using TCB as the processing solvent. A similar trend is also found in the FETs based on **P4TTT**. It suggests that the high boiling-point solvents significantly improves the molecular packing and facilitates the formation of the nanofiber morphology, leading to the high charge mobilities.

The **P4TDTT** FETs showed hole mobilities much higher than the **P4TTT** FETs prepared from TCB. The higher FET mobility of **P4TDTT** than that of **P4TTT** is likely due to the influence of the conjugated side chains and the core size of fused-thiophene moieties. The nonsymmetry arrangement of conjugated side chains on **P4TDTT** lead to a larger dipole moment (2.1506 D), contributing to a stronger intermolecular interaction and a denser $\pi-\pi$ stacking distance (3.56 Å). Furthermore, the **P4TDTT** film has the higher density of crystalline nanofibers compared to **P4TTT**, which provides effective pathways for charge transport. Even though **P4TDTT** showed a higher mobility, **P4TDTT** exhibited a lower degree of lamellar ordering, as evident from weaker (200) and (300) diffraction peaks. This presents some possibility that the hole mobilities of **P4TDTT** may be further enhanced if the better lamellar ordering could be improved through slower solvent evaporation or solvent annealing.

Figure 9 shows the air stability testing of **P4TDTT** and **P4TTT** FETs obtained by measuring the variation of hole mobilities with time in air. In contrast to the dramatic degradation in the mobilities of the P3HT FETs,[13] the FETs of **P4TDTT** and **P4TTT** exhibit a high air stability. The average mobilities of **P4TDTT** and **P4TTT** are slightly decreased from 0.56 and 0.30 $cm^2\ V^{-1}\ s^{-1}$ to 0.37 and 0.24 $cm^2\ V^{-1}\ s^{-1}$, respectively, after being stored in air for 8 days (humidity level: 50−60%). Even after being stored in the air for four months, the average FET hole mobilities of **P4TDTT** and **P4TTT** still have the high mobilities of 0.34 and 0.23 $cm^2\ V^{-1}\ s^{-1}$, respectively, showing a slow degradation for charge transport in air. The on−off ratios was decreased to 10^3, because of an increase of OFF currents, probably attributed to the influence of humidity, enhancing the leakage current of devices.[39] Intriguingly, the threshold voltages of these devices were slightly shifted to 3 V, after being stored in the air for four months, indicating the excellent oxidative resistance in air. Note that P3HT exhibited a large degradation of charge mobilities about 2 orders of magnitude when stored in air.[13] The great stability of **P4TDTT** and **P4TTT** is likely due to the fact that the attachment of the conjugated side chains into the main chains increases steric hindrance, lowing the HOMO levels and thus improving ambient stability.[18] It should be noted that **P4TTT** exhibited a better air stability, compared to **P4TDTT**, as

a result of the slightly lower-lying HOMO level of the former. These results indicate that biaxially extended conjugated polythiophenes have potential applications for high-performance air-stable FETs.

CONCLUSIONS

We have studied the synthesis, morphology and charge transport characteristics of the biaxially extended thiophene-fused thiophene containing conjugated copolymers, **P4TDTT** and **P4TTT**. The results revealed that the combination of coplanar fused thiophene rings and conjugated side chains could improve charge transport and air stability of FETs. **P4TDTT** exhibited a high field effect mobility of up to 0.61 $cm^2 V^{-1} s^{-1}$ and on/off ratios ranged from 10^5 to 10^6. The FET performance of **P4TDTT** is higher than that of **P4TTT**, due to the non-symmetry side-chain arrangement and larger coplanar moieties of the former, leading to an enhanced interchain interaction and denser molecular packing. Furthermore, the FETs of the polymers showed great air stability, even after being stored in the air for four months. These results demonstrate that the biaxially extended thiophene based conjugated copolymers, **P4TDTT** and **P4TTT**, are promising materials for high-performance air-stable solution-processable organic FET devices.

ASSOCIATED CONTENT

Supporting Information. ^{1}H NMR spectra of **P4TTT**, TGA curves of studied copolymers at a heating rate of 10 °C min^{-1} under a nitrogen atmosphere, TEM images of the thin films of the polymers prepared from CF, CB, and DCB, and AFM height images of the thin films prepared from TCB. This material is available free of charge via the Internet at http://pubs.acs.org.

AUTHOR INFORMATION

Corresponding Author

*E-mail:chenwc@ntu.edu.tw.

Author Contributions

§Equally contributed to the work.

ACKNOWLEDGMENT

The financial support from National Science Council of Taiwan and National Taiwan University Excellent Research program are highly appreciated. We thank Professor S. H. Tung for the helpful discussion on the XRD and Dr. Jung-Ching Hsu for the technical assistance of TEM images.

REFERENCES

(1) Allard, S.; Forster, M.; Souharce, B.; Thiem, H.; Scherf, U. *Angew. Chem., Int. Ed.* **2008**, *47*, 4070.
(2) Arias, A. C.; MacKenzie, J. D.; McCulloch, I.; Rivnay, J.; Salleo, A. *Chem. Rev.* **2010**, *110*, 3.
(3) Bao, Z.; Locklin, J. *Organic field-effect transistors*; CRC Press: Boca Raton, FL, 2007.
(4) Guo, Y.; Yu, G.; Liu, Y. *Adv. Mater.* **2010**, *22*, 4427.
(5) Klauk, H. *Chem. Soc. Rev.* **2010**, *39*, 2643.
(6) Sun, J.; Zhang, B.; Katz, H. E. *Adv. Funct. Mater* **2011**, *21*, 29.
(7) Wen, Y.; Liu, Y.; Guo, Y.; Yu, G.; Hu, W. *Chem. Rev.* **2011**, *111*, 3358.
(8) Yan, H.; Chen, Z.; Zheng, Y.; Newman, C.; Quinn, J. R.; Dötz, F.; Kastler, M.; Facchetti, A. *Nature* **2009**, *457*, 679.
(9) Zaumseil, J.; Sirringhaus, H. *Chem. Rev.* **2007**, *107*, 1296.
(10) Bao, Z.; Lovinger, A. J.; Dodabalapur, A. *Appl. Phys. Lett.* **1996**, *69*, 3066.
(11) Sirringhaus, H. *Science* **1998**, *280*, 1741.
(12) Sirringhaus, H.; Brown, P. J.; Friend, R. H.; Nielsen, M. M.; Bechgaard, K.; Langeveld-Voss, B. M. W.; Spiering, A. J. H.; Janssen, R. A. J.; Meijer, E. W.; Herwig, P.; de Leeuw, D. M. *Nature* **1999**, *401*, 685.
(13) Schafferhans, J.; Baumann, A.; Deibel, C.; Dyakonov, V. *Appl. Phys. Lett.* **2008**, *93*, 093303.
(14) Asadi, K.; Gholamrezaie, F.; Smits, E. C. P.; Blom, P. W. M.; Boer, B. d. *J. Mater. Chem.* **2007**, *17*, 1947.
(15) Ong, B. S.; Wu, Y.; Liu, P.; Gardner, S. *J. Am. Chem. Soc.* **2004**, *126*, 3378.
(16) Zhang, W. M.; Smith, J.; Watkins, S. E.; Gysel, R.; McGehee, M.; Salleo, A.; Kirkpatrick, J.; Ashraf, S.; Anthopoulos, T.; Heeney, M.; McCulloch, I. *J. Am. Chem. Soc.* **2010**, *132*, 11437.
(17) Murphy, A. R.; Liu, J.; Luscombe, C.; Kavulak, D.; Frechet, J. M. J.; Kline, R. J.; McGehee, M. D. *Chem. Mater.* **2005**, *17*, 4892.
(18) Park, J. W.; Lee, D. H.; Chung, D. S.; Kang, D. M.; Park, C. E.; Kwon, S. K. *Macromolecules* **2010**, *43*, 2118.
(19) Tsai, J.-H.; Lee, W.-Y.; Chen, W.-C.; Yu, C.-Y.; Hwang, G.-W.; Ting, C. *Chem. Mater.* **2010**, *22*, 3290.
(20) Yu, C.-Y.; Ko, B.-T.; Ting, C.; Chen, C.-P. *Sol. Energy Mater. Sol. Cells* **2009**, *93*, 613.
(21) Zhou, E. J.; Tan, Z. A.; Huo, L. J.; He, Y. J.; Yang, C. H.; Li, Y. F. *J. Phys. Chem. B* **2006**, *110*, 26062.
(22) Li, Y.; Singh, S. P.; Sonar, P. *Adv. Mater.* **2010**, *22*, 4862.
(23) Li, Y. N.; Wu, Y. L.; Liu, P.; Birau, M.; Pan, H. L.; Ong, B. S. *Adv. Mater.* **2006**, *18*, 3029.
(24) Lim, E.; Lee, S.; Lee, K. K. *Mol. Cryst. Liq. Cryst.* **2011**, *538*, 157.
(25) Chua, L. L.; Zhuo, J. M.; Zhao, L. H.; Png, R. Q.; Wong, L. Y.; Chia, P. J.; Tang, J. C.; Sivaramakrishnan, S.; Zhou, M.; Ou, E. C. W.; Chua, S. J.; Sim, W. S.; Ho, P. K. H. *Adv. Mater.* **2009**, *21*, 4747.
(26) DeLongchamp, D. M.; Kline, R. J.; Jung, Y.; Lin, E. K.; Fischer, D. A.; Gundlach, D. J.; Cotts, S. K.; Moad, A. J.; Richter, L. J.; Toney, M. F.; Heeney, M.; McCulloch, I. *Macromolecules* **2008**, *41*, 5709.
(27) Di, C.-a.; Lu, K.; Zhang, L.; Liu, Y.; Guo, Y.; Sun, X.; Wen, Y.; Yu, G.; Zhu, D. *Adv. Mater.* **2010**, *22*, 1273.
(28) Gather, M. C.; Heeney, M.; Zhang, W. M.; Whitehead, K. S.; Bradley, D. D. C.; McCulloch, I.; Campbell, A. J. *Chem. Commun.* **2008**, 1079.
(29) He, M.; Li, J.; Sorensen, M. L.; Zhang, F.; Hancock, R. R.; Fong, H. H.; Pozdin, V. A.; Smilgies, D.-M.; Malliaras, G. G. *J. Am. Chem. Soc.* **2009**, *131*, 11930.
(30) He, Y. J.; Wu, W. P.; Zhao, G. J.; Liu, Y. Q.; Li, Y. F. *Macromolecules* **2008**, *41*, 9760.
(31) Heeney, M.; Bailey, C.; Genevicius, K.; Shkunov, M.; Sparrowe, D.; Tierney, S.; McCulloch, I. *J. Am. Chem. Soc.* **2005**, *127*, 1078.
(32) Hwang, I. W.; Kim, J. Y.; Cho, S.; Yuen, J.; Coates, N.; Lee, K.; Heeney, M.; McCulloch, I.; Moses, D.; Heeger, A. J. *J. Phys. Chem. C* **2008**, *112*, 7853.
(33) Kong, H.; Lee, D. H.; Kang, I. N.; Lim, E.; Jung, Y. K.; Park, J. H.; Ahn, T.; Yi, M. H.; Park, C. E.; Shim, H. K. *J. Mater. Chem.* **2008**, *18*, 1895.
(34) Leclerc, N.; Biniek, L.; Fall, S.; Chochos, C. L.; Anokhin, D. V.; Ivanov, D. A.; Leveque, P.; Heiser, T. *Macromolecules* **2010**, *43*, 9779.
(35) Li, C. M.; Li, J.; Qin, F.; Bao, Q. L.; Chan-Park, M. B.; Zhang, W.; Qin, J. G.; Ong, B. S. *Chem. Mater.* **2008**, *20*, 2057.
(36) Li, J.; Tan, H.-S.; Chen, Z.-K.; Goh, W.-P.; Wong, H.-K.; Ong, K.-H.; Liu, W.; Li, C. M.; Ong, B. S. *Macromolecules* **2011**, *44*, 690.
(37) Liu, Y.; Liu, Y.; Zhan, X. *Macromol. Chem. Phys.* **2011**, *212*, 428.
(38) Mas-Torrent, M.; Rovira, C. *Chem. Soc. Rev.* **2008**, *37*, 827.
(39) McCulloch, I.; Heeney, M.; Bailey, C.; Genevicius, K.; MacDonald, I.; Shkunov, M.; Sparrowe, D.; Tierney, S.; Wagner, R.; Zhang, W.; Chabinyc, M. L.; Kline, R. J.; McGehee, M. D.; Toney, M. F. *Nat. Mater.* **2006**, *5*, 328.
(40) McCulloch, I.; Heeney, M.; Chabinyc, M. L.; DeLongchamp, D.; Kline, R. J.; Cölle, M.; Duffy, W.; Fischer, D.; Gundlach, D.;

Hamadani, B.; Hamilton, R.; Richter, L.; Salleo, A.; Shkunov, M.; Sparrowe, D.; Tierney, S.; Zhang, W. *Adv. Mater.* **2009**, *21*, 1091.
(41) Miguel, L. S.; Matzger, A. J. *Macromolecules* **2007**, *40*, 9233.
(42) Milian Medina, B.; Van Vooren, A.; Brocorens, P.; Gierschner, J.; Shkunov, M.; Heeney, M.; McCulloch, I.; Lazzaroni, R.; Cornil, J. *Chem. Mater.* **2007**, *19*, 4949.
(43) Pron, A.; Gawrys, P.; Zagorska, M.; Djurado, D.; Demadrille, R. *Chem. Soc. Rev.* **2010**, *39*, 2577.
(44) Sun, Q. J.; Park, K.; Dai, L. M. *J. Phys. Chem. C* **2009**, *113*, 7892.
(45) Tang, W. H.; Ke, L.; Tan, L. W.; Lin, T. T.; Kietzke, T.; Chen, Z. K. *Macromolecules* **2007**, *40*, 6164.
(46) Wu, W. P.; Liu, Y. Q.; Zhu, D. B. *Chem. Soc. Rev.* **2010**, *39*, 1489.
(47) Zhang, X. R.; Hudson, S. D.; DeLongchamp, D. M.; Gundlach, D. J.; Heeney, M.; McCulloch, I. *Adv. Funct. Mater* **2010**, *20*, 4098.
(48) Kim, K. H.; Chung, D. S.; Park, C. E.; Choi, D. H. *J. Polym. Sci., Part A: Polym. Chem.* **2011**, *49*, 55.
(49) Frey, J.; Bond, A. D.; Holmes, A. B. *Chem. Commun.* **2002**, 2424.
(50) Zhan, X. W.; Tan, Z. A.; Domercq, B.; An, Z. S.; Zhang, X.; Barlow, S.; Li, Y. F.; Zhu, D. B.; Kippelen, B.; Marder, S. R. *J. Am. Chem. Soc.* **2007**, *129*, 7246.
(51) Frisch, M. J., Trucks, G. W.; Schlegel, H. B.; Scuseria, G. E.; Robb, M. A.; Cheeseman, J. R., Montgomery , J. A., Jr.; Vreven, T.; Kudin, K. N. Burant, J. C.; Millam, J. M.; Iyengar, S. S.; Tomasi, J.; Barone, V.; Mennucci, B.Cossi, M.; Scalmani, G.; Rega, N.; Petersson, G. A. Nakatsuji, H.; Hada, M.; Ehara, M.; Toyota, K.; Fukuda, R. Hasegawa, J.; Ishida, M.; Nakajima, T.; Honda, Y.; Kitao, O. Nakai, H.; Klene, M.; Li, X.; Knox, J. E.; Hratchian, H. P.; Cross, J. B., Bakken, V.; Adamo, C.; Jaramillo, J.; Gomperts, R.; Stratmann, R. E. Yazyev, O.; Austin, A. J.; Cammi, R.; Pomelli, C. Ochterski, J. W.; Ayala, P. Y.; Morokuma, K.; Voth, G. A. Salvador, P.; Dannenberg, J. J.; Zakrzewski, V. G.; Dapprich, S. Daniels, A. D.; Strain, M. C.; Farkas, O.; Malick, D. K.; Rabuck, A. D. Raghavachari, K.; Foresman, J. B.; Ortiz, J. V.; Cui, Q. Baboul, A. G.; Clifford, S.; Cioslowski, J.; Stefanov, B. B.; Liu, G. Liashenko, A.; Piskorz, P.; Komaromi, I.; Martin, R. L.; Fox, D. J. Komaromi, T.; Al-Laham, M. A.; Peng, C. Y.; Nanayakkara, A. Challacombe, M.; Gill, P. M. W.; Johnson, B.; Chen, W. W., M. W.; Gonzalez, C.; Pople, J. A. *Gaussian 03 revision B.04* Gaussian, Inc.: Wallingford, CT, 2004.
(52) Liu, C. L.; Tsai, J. H.; Lee, W. Y.; Chen, W. C.; Jenekhe, S. A. *Macromolecules* **2008**, *41*, 6952.
(53) Lee, W. Y.; Cheng, K. F.; Wang, T. F.; Chueh, C. C.; Chen, W. C.; Tuan, C. S.; Li, J. L. *Macromol. Chem. Phys.* **2007**, *208*, 1919.
(54) de Leeuw, D. M.; Simenon, M. M. J.; Brown, A. R.; Einerhand, R. E. F. *Synth. Met.* **1997**, *87*, 53.
(55) Zhu, Y.; Champion, R. D.; Jenekhe, S. A. *Macromolecules* **2006**, *39*, 8712.
(56) Chang, J.-F.; Sun, B.; Breiby, D. W.; Nielsen, M. M.; Sölling, T. I.; Giles, M.; McCulloch, I.; Sirringhaus, H. *Chem. Mater.* **2004**, *16*, 4772.
(57) Tsao, H. N.; Mullen, K. *Chem. Soc. Rev.* **2010**, *39*, 2372.
(58) Letizia, J. A.; Salata, M. R.; Tribout, C. M.; Facchetti, A.; Ratner, M. A.; Marks, T. J. *J. Am. Chem. Soc.* **2008**, *130*, 9679.
(59) Tsao, H. N.; Cho, D. M.; Park, I.; Hansen, M. R.; Mavrinskiy, A.; Yoon, D. Y.; Graf, R.; Pisula, W.; Spiess, H. W.; Müllen, K. *J. Am. Chem. Soc.* **2011**, *133*, 2605.
(60) Kim, D. H.; Jang, Y.; Park, Y. D.; Cho, K. *J. Phys. Chem. B* **2006**, *110*, 15763.
(61) Qiu, L.; Lee, W. H.; Wang, X.; Kim, J. S.; Lim, J. A.; Kwak, D.; Lee, S.; Cho, K. *Adv. Mater.* **2009**, *21*, 1349.